Received: 3 September 2019 | Revised: 23 October 2019 | Accepted: 23 October 2019

DOI: 10.1111/jace.16881

ORIGINAL ARTICLE

Journal of the American Ceramic Society

High temperature creep-mediated functionality in polycrystalline barium titanate

Pengrong Ren[1,2] | **Marion Höfling**[2] | **Jurij Koruza**[2] | **Stefan Lauterbach**[2] | **Xijie Jiang**[2] | **Till Frömling**[2] | **Dipak Kumar Khatua**[3] | **Christian Dietz**[2] | **Lukas Porz**[2] | **Rajeev Ranjan**[3] | **Hans-Joachim Kleebe**[2] | **Jürgen Rödel**[2]

[1]Shaanxi Province Key Laboratory for Electrical Materials and Infiltration Technology, Department of Materials Science and Engineering, Xi'an University of Technology, Xi'an, China

[2]Institute of Materials Science, Technische Universität Darmstadt, Darmstadt, Germany

[3]Department of Materials Engineering, Indian Institute of Science, Bangalore, India

Correspondence
Marion Höfling, Institute of Materials Science, Technische Universität Darmstadt, Alarich-Weiss-Straße 2, 64287 Darmstadt, Germany.
Email: hoefling@ceramics.tu-darmstadt.de

Funding information
Deutsche Forschungsgemeinschaft, Grant/Award Number: 398795637; National Natural Science Foundation, Grant/Award Number: 51972265; Key Research and Development Program, Grant/Award Number: 2019KW and -025

Abstract

Dislocations in oxides can be described as charged line defects and means for one-dimensional doping, which can tune electrical and thermal properties. Furthermore, theoretically it was shown that dislocations can pin ferroelectric domain walls. Broader application of this concept hinges on the development of a methodology to avail this approach to polycrystalline ceramics. To this end, we use different creep mechanisms as a method to introduce multidimensional defects and quantify structural changes. A deformation map for fine-grained barium titanate is provided and the influences of the defects and creep regimes are correlated in this first study to modifications of electrical conductivity, dielectric, ferroelectric, and piezoelectric properties. A plastic deformation of 1.29% resulted in an increase in the Curie temperature by 5°C and a decrease in electromechanical strain by 30%, pointing toward electromechanical hardening by dislocations.

KEYWORDS

barium titanate, creep, dislocations, ferroelectricity/ferroelectric materials, piezoelectric materials/properties

1 | INTRODUCTION

Functional properties of materials can be tailored using 0-dimensional (point defects), 1-dimensional (dislocations), 2-dimensional (interfaces), and 3-dimensional (precipitates, second-phase particles, and pores) defects.[1] In functional materials, a strong emphasis is placed on acceptor-, donor-, or isovalent doping with the attendant disadvantage that induced mobile point defects may incur limited temperature stability or stability with respect to high electric fields, as, for example, in high-power materials.[2] While the influence of grain boundaries[3] or secondary phases on the properties is discussed in literature, there is still a lack of knowledge about 1-dimensional doping, especially in the field of electroceramics such as piezo- and ferroelectrics. For 3-dimensional defects Lalitha et al[4] investigated the influence of second-phase hardening as an approach to harden ferroelectrics. A recently described design concept,

Pengrong Ren and Marion Höfling contributed equally to this work.

1-dimensional doping,[5] utilizes charged dislocations[6] to impact properties of oxides.[7] This approach has demonstrated large changes in conductivity in plastically deformed TiO_2 and $SrTiO_3$ single crystals. [8–10] Similarly, dislocations have been proven to pin flux lines in superconductors[11] and to enhance the thermoelectric figure of merit by reducing thermal conductivity.[12] In ferroelectrics, theoretical work has suggested that dislocations can pin domain walls[13] and, hence, should be able to influence dielectric losses for high-power applications.[14] The applicability of the 1-dimensional doping concept,[8] however, hinges on availability of single crystals, which can be deformed.[9] Dislocations on a small scale can be introduced by indentation[15,16] or surface treatments, but with these methods macroscopical changes in the ferroelectric properties cannot be reached. While recent fundamental work by Ohsima et al[17] demonstrated that changes in illumination provide drastic changes in ductility of semiconductors, this may not be possible for ceramics in general. To this end, further development and usage of the concept of 1-dimensional doping, which is the purposeful introduction of charged dislocations into ceramics, hinges on a methodology to introduce dislocations in a controlled manner into polycrystalline ceramics. If successful, this could open a new design tool for functional ceramics in general.

This work is designed to provide a general methodology to utilize high temperature creep to introduce dislocations—or in general defects—in a controlled manner and consequently to alter functional properties of oxides. Creep describes the time-dependent deformation of a material at constant stress and can be divided into two main categories: the diffusion creep at low stresses and the dislocation creep at high stresses.[18] Diffusion creep is driven by a gradient of chemical potential of vacancies between different stressed regions, for example, grain boundaries. Tensile stress at the grain boundary assists the vacancy formation, while compressive stress leads to a decrease in vacancy concentration. The resulting gradient in vacancy concentration is the driving force for diffusion.[19] Depending on the diffusional path, creep can be separated into Coble creep (along the grain boundaries)[20] and Nabarro-Herring creep (through the lattice).[21,22] Both processes are grain size dependent. In contrast to this, the climb and glide processes of dislocations in the dislocation creep regime are intragranular processes and therefore independent of grain size.[18] Additionally, grain-boundary sliding can have a significant contribution to the creep strain due to cavitation and void formation and can therefore also be classified as damage-enhanced creep.[23–25] The creep studies in this work are built on prior studies in structural materials at the end of the 20th century when creep deformation maps were constructed and different creep mechanisms were distinguished.[26–31]

This work outlines an approach to delineate different creep regimes and offers tools to investigate changes to the microstructure, which will be correlated with changes observed in electrical conductivity, dielectric, ferroelectric, and piezoelectric properties. For this first study, the prototype ferroelectric $BaTiO_3$ was chosen as the model material.[32]

2 | EXPERIMENTAL PROCEDURE

$BaTiO_3$ powder was prepared via conventional solid-state reaction using TiO_2 (purity ≥99.6%, Sigma-Aldrich, St Louis, USA) and $BaCO_3$ (purity ≥99.8%, Sigma-Aldrich, St Louis, USA) as raw materials. The powders were mixed according to the stoichiometric formula and ball-milled for 12 hours with zirconia balls and ethanol in a planetary ball mill (Fritsch Pulverisette 5, Idar-Oberstein, Germany). After drying and calcination at 1100°C for 6 hours they were re-milled for 24 hours. A die with an inner diameter of 6.5 mm was employed to press samples of cylindrical shape. The green cylinders were further compacted under 200 MPa using a cold isostatic press (KIP 100E, Weber, Remshalden, Germany). Specimens were sintered at 1350°C for 6 hours yielding cylinders with a diameter of about 4.8 mm and a height of 16.5 mm. In the next step, these were cut into two smaller cylinders (9.5 mm and 7 mm height) using a diamond wire saw. Both parts were further reduced to 4 mm ± 0.05 mm in diameter using a lathe. Samples were ground plan parallel, in order to minimize the friction between the cylinder and the compression loading rods and to ensure a homogeneous stress distribution during plastic deformation. Finally, cylinders with dimensions of 4 mm ± 0.05 mm in diameter and 8 mm ± 0.02 mm in height were used for the creep experiments. The smaller reference cylinder was cut into pellets (labelled as undeformed BT). The schematics in Figure 1 illustrate the sample preparation process.

Creep studies were performed in two steps. The first step served to distinguish the regimes of different creep mechanisms and to construct the deformation map,[8] while the second step was performed to manufacture samples deformed at a defined stress and temperature to investigate the influence of a certain creep regime.

For the deformation map, creep experiments were carried out above $0.5 \cdot T_m$,[28], that is, at 950°C, 1000°C, 1050°C, and 1100°C, with a step-wise increase in the uniaxial compressive stress from 100 MPa to 225 MPa at intervals of 25 MPa, as displayed in Figure 2. These experiments were carried out using a screw-driven load frame (Z010, Zwick GmbH & Co. KG, Ulm, Germany) with an attached furnace (LK/SHC 1500-85-150-1-V-Sonder, HTM Reetz GmbH, Berlin, Germany). The displacement of the $BaTiO_3$ cylinders was quantified with a linear variable differential transducer (LVDT).

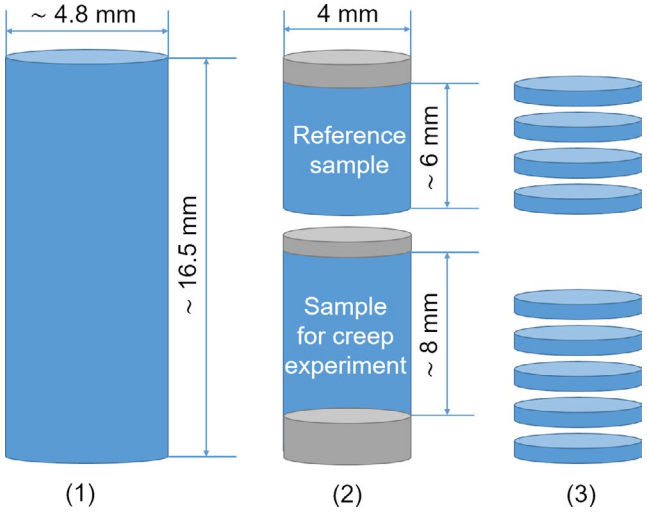

FIGURE 1 Outline of the samples used in this study. The sintered cylinder (1) was cut in two smaller parts (2), whereby one was deformed and the other served as a reference (the edges marked with gray were discarded). For characterization and electrical measurements the cylinders were cut into small discs (3) [Color figure can be viewed at wileyonlinelibrary.com]

The range of stress values was chosen to determine the exponents in the power law creep equation as the key measure to distinguish between different creep regimes. The cylinders were placed in between two alumina rods. During heating (5 K/min), a constant load of approximately 1.6 MPa (20 N) was applied to avoid damage of the sample due to thermal expansion of the setup. Thermal equilibrium was then established by holding the sample for 30 minutes at the maximum temperature. The compressive stress was applied with a loading rate of 1 MPa/s and held at each load interval for 30 minutes. After the final deformation step, the stress was released to 1.6 MPa. With this load maintained, the sample cooled down to room temperature. Muñoz-Saldaña et al[33] suggested that the critical stress for initiating domain switching in single crystalline barium titanate is 6 MPa. Later in the results it is additionally verified that there are no significant changes in domain size for the undeformed and deformed samples, therefore it is assumed that the stress during cooling below the Curie temperature can be neglected.

In the second step, cylinders were deformed at fixed temperature, compressive stress, and time, respectively, to capture either diffusion creep or dislocation creep. The loading schemes were chosen as a compromise between introducing a high density of dislocations[27] and avoiding microstructural damage like extensive cavitation or crack formation.

One sample was deformed at 1000°C and 200 MPa for 15 minutes (labelled as C-1000°C-15 min), while the others were deformed at 1050°C and 200 MPa for 15, 22, and 30 minutes, (samples are labelled C-1050°C-15 min, C-1050°C-22 min, and C-1050°C-30 min, respectively). Time spans of at least 15 minutes were selected to enter the steady-state creep regime. According to Blum et al[27] the steady-state creep regime is characterized by a dynamic equilibrium, after an increase in the dislocation density in the primary regime. In order to minimize recovery of dislocations and their annihilation by dipole elimination during the cooling process,[27] the compressive stress was maintained until the temperature decreased to 1000°C and was afterward reduced to 1.6 MPa. After the creep experiments, cylinders were cut into several pellets with a thickness of

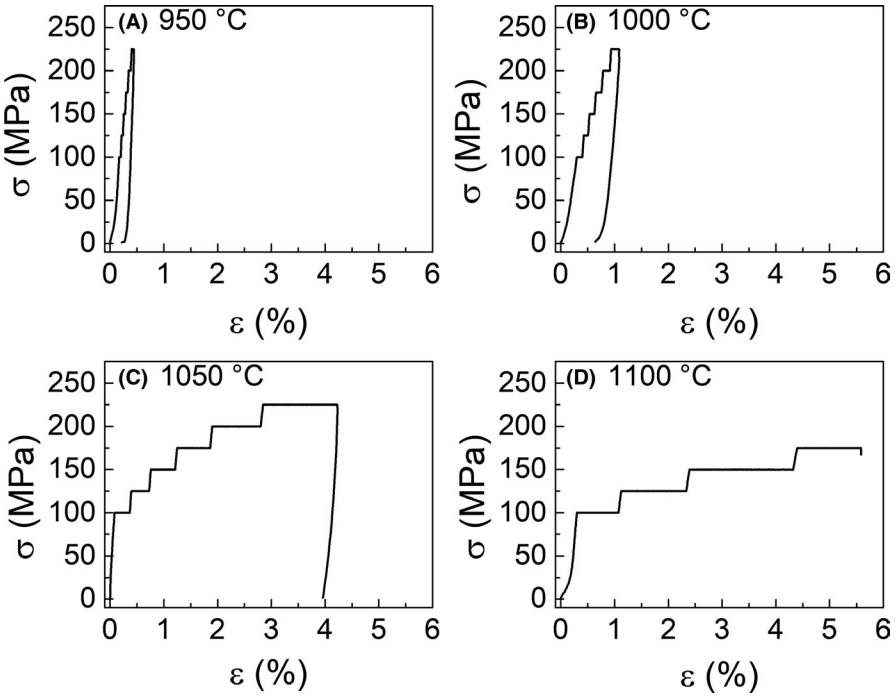

FIGURE 2 Stress-strain curves for the different temperatures are displayed in (A) at 950°C, (B) at 1000°C, (C) at 1050°C, and (D) at 1100°C. The plateaus of the stress steps were used to identify the creep regimes. For both the compressive stress and the negative strain the absolute values are given

about 1 mm for further characterization and electrical measurements (Figure 1).

The density of the sintered pellets and creeped samples was obtained with the Archimedes' immersion method, while the elastic modulus was quantified by acoustic emission using a thickness gauge. The microstructure was quantified from polished cross sections after thermal etching at 1250°C for 10 minutes using scanning electron microscopy (SEM) (XL30FEG, Philips, Amsterdam, Netherlands).

Both the undeformed and the deformed $BaTiO_3$ were ground to a thickness of 0.8 mm and sputtered with Pt for electrical measurements. The temperature-dependent dielectric permittivity (ε') and dielectric loss (tanδ) were determined with an LCR meter (HP 4284A, HewlettPackard Corporation, Palo Alto, CA, USA) from 20°C to 250°C (2 K/min) using frequencies of 1 kHz, 10 kHz, 100 kHz, and 1 MHz with an amplitude of 0.5 V/mm. The polarization- and electrostrain-hysteresis measurements were performed at 10 Hz using a modified Sawyer-Tower circuit and an integrated optical sensor. Impedance spectroscopy (IS) was applied using an impedance analyzer (alpha-Analyzer, Novocontrol Technologies, Hundsangen, Germany) from 700°C to 300°C (cooling process) with an amplitude of 0.1 V/mm and a measuring frequency range from 0.1 Hz to 3 MHz. The domain structure of polished surfaces was obtained with a piezoresponse force microscope (PFM) (MPF-3D, Asylum Research, Santa Barbara, CA, USA). The microstructural changes caused by the creep experiments were imaged using transmission electron microscopy (TEM) (FEI CM20 ST, FEI, Eindhoven, Netherlands) operated at 200 kV accelerating voltage. For this purpose, the samples were prepared by grinding, cutting, dimpling, and ion milling. The dimpled disks were annealed at 200°C for 2 hours to minimize any artifacts that may have been introduced during mechanical thinning. The microstrain of the ceramics were determined by X-ray diffraction (XRD) using a Rigaku Smartlab X-ray diffractometer with a HT attachment (Anton Paar, Graz, Austria). A Cu-$K_{\alpha 1}$ monochromatic X-ray beam with power 9 kW, step size 0.01°, angle range 20°-85° and scan speed 1.5 °/min was used for the experiment. Microstrain analysis was done by calculating the full width at half maxima (FWHM) of $\{200\}_{pc}$ XRD Bragg peaks of specimens in the temperature interval from 150°C to 400°C. The peak position was quantified from room temperature up to 150°C.

3 | RESULTS AND DISCUSSION

3.1 | Development of a creep deformation map

At first, step-wise creep experiments, depicted in Figure 2, were carried out to obtain the creep deformation map of polycrystalline $BaTiO_3$. To this end, steady-state creep must be reached to apply the power law creep equation. At the same time microcracking and grain growth should be avoided. Therefore, first the true strain ε was calculated according to Equation (1):[34]

$$\varepsilon = -\ln\left(1-\left(\frac{dl}{l_0}\right)\right) \tag{1}$$

with the initial height of the sample l_0 and the change in the sample height dl during the creep experiment.[35]

In Figure 3A strain as function of time is featured for the first deformation step at 100 MPa (1050°C). Above a strain of 0.15% the slope of the strain curve becomes constant, which indicates that the steady-state creep regime is reached. The first creep regime was only clearly visible in the first applied stress level during the creep experiments. In Figure 3B the linear range is displayed for the creep range at 200 MPa. An alternative approach utilizes a presentation of strain rate as function of strain.[35] This is depicted in Figure 3C where the stress range for 100 MPa and 200 MPa is highlighted in color for the step-wise creep experiment at 1050°C. With the proof that the strain rate $\dot{\varepsilon}$ is constant and the steady state creep regime is reached, the power law Equation (2) can be applied,

$$\dot{\varepsilon} = A\sigma^n \exp\left(-\frac{Q}{RT}\right) \tag{2}$$

where n is the stress exponent, Q is the activation energy, R is the gas constant (8.31 J mol^{-1} K^{-1}), T is the temperature, and A is a constant.[35] This equation is applicable for constant grain size,

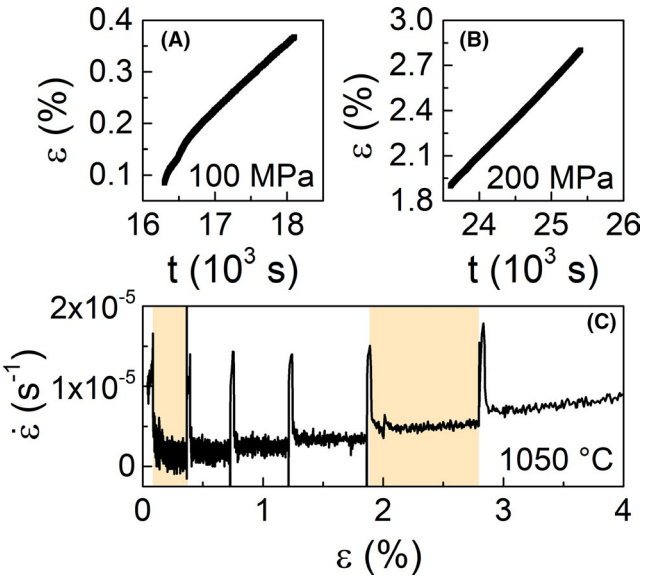

FIGURE 3 Creep strain as function of time for (A) 100 MPa and (B) 200 MPa at 1050°C. (C) strain rate as function of strain for the whole stress step function. Ranges for the compressive stress of 100 MPa and 200 MPa are highlighted. The creep strain is given in absolute values [Color figure can be viewed at wileyonlinelibrary.com]

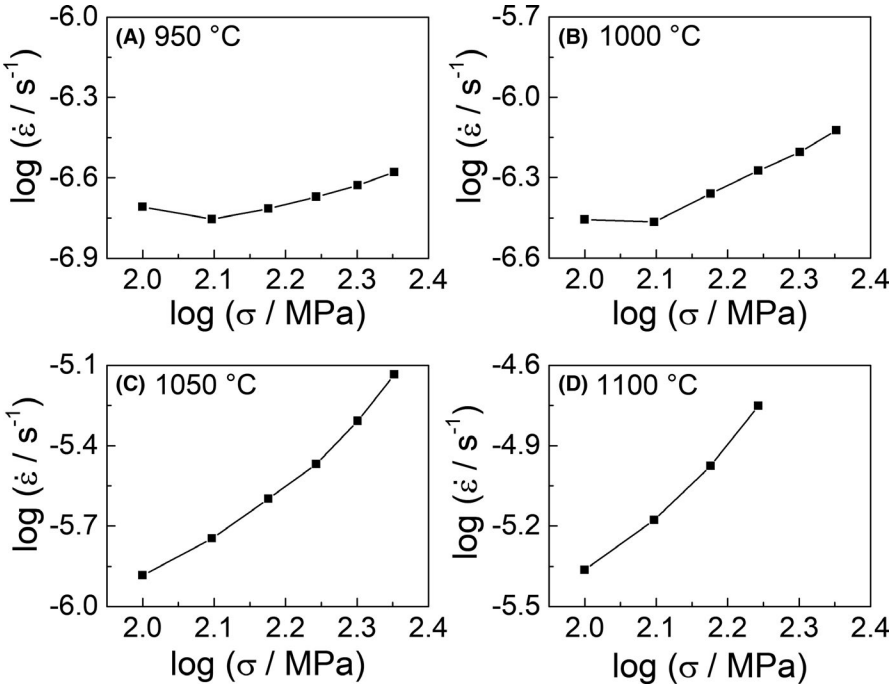

FIGURE 4 Strain rate as function of compressive stress to determine the stress exponent at (A) 950°C, (B) 1000°C, (C) 1050°C, and (D) 1100°C

which will be verified in Chapter II. According to Equation (2), n can be calculated from the slope of $\log(\dot{\varepsilon})$ and $\log(\sigma)$ (Figure 4), if T is constant and Q is assumed to be independent of σ.

The stress exponent was calculated between each of the two data points. For a simplified representation, the stress values given in the deformation map correspond to the mean value of the two applied stresses. Furthermore, the stress exponents were classified in the following ranges: $0 < n < 1$ (linear regime), $1 \leq n < 3$ (diffusion creep regime[29]), and $n \geq 3$ (dislocation creep regime [28]). Note that for the creep deformation map grain-boundary sliding was neglected. Grain-boundary sliding can appear at all stress levels and is therefore a parallel process to both diffusion and dislocation creep.[25] This phenomenon will be further discussed later in the microstructure analysis. The first data point in Figure 4A,B is neglected due to the negative stress exponent between the first and second data point. A negative exponent indicates that the second creep regime is not reached for this stress-temperature level. Finally, the different creep regimes, given in Figure 5, are colored for the linear regime (squares) in green, for the diffusion creep regime (circles) in yellow, and for dislocation creep regime (triangles) in blue. As expected, with increasing stress and temperature the stress exponents increase.

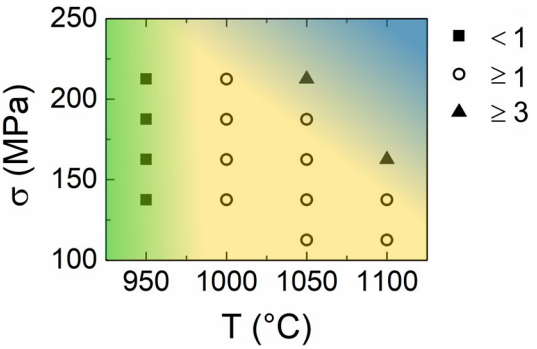

FIGURE 5 Creep deformation for different compressive stresses and different temperatures. The square data points represent stress exponents below 1 (elastic), circles a stress exponent between 1 and 3 (diffusion range), and triangles above 3 (dislocation creep), respectively. The green (elastic), yellow (diffusion), and blue (dislocation) areas indicate the different creep regimes in fine-grained $BaTiO_3$ [Color figure can be viewed at wileyonlinelibrary.com]

3.2 | Creep-induced changes in the microstructure, dielectric, and ferroelectric properties

Based on the deformation map (Figure 5), individual stress-temperature combinations were chosen to investigate the influence of the diffusion and dislocation creep regimes on the microstructural features, as well as the dielectric, piezoelectric, and ferroelectric properties. Prior experiments suggested that the total plastic strain should be kept below 2.5% to avoid microcracks and failure. Therefore, the time span was limited to 30 minutes.

Values for the relative density, the elastic modulus, the total creep strain (plastic strain), and the grain size are summarized in Table 1. Figure 6 displays the SEM images for the undeformed BT, C-1000°C-15 min, and C-1050°C-30 min samples. All samples have an average grain size between 1.4 μm ± 0.4 μm for the undeformed and 1.9 μm ± 1.0 μm for the C-1050°C-30 min sample,

Sample	ρ (g/cm^3)	ρ_{rel} (%)	E (GPa)	ε_{def} (%)	G (μm)
Undeformed BT	5.71	94.9	114.7	0	1.4 ± 0.4
C-1000°C-15 min	5.68	94.4	119.0	0.29	1.7 ± 0.8
C-1050°C-15 min	5.90	97.9	126.5	0.60	1.8 ± 0.9
C-1050°C-22 min	5.75	95.5	117.6	1.06	1.7 ± 0.8
C-1050°C-30 min	5.55	92.1	113.5	1.29	1.9 ± 1.0

TABLE 1 Absolute (ρ) and relative densities (ρ_{rel}), elastic modulus (E), creep strain (plastic strain, ε_{def}), and grain size (G) for undeformed and deformed BT at different conditions

whereby the changes between the samples are in the range of the standard deviation. $BaTiO_3$ has a tendency to exhibit twinning during sintering[36] and a higher density of twins may affect functional properties as well. The density of twins was determined from SEM images (marked in Figure 6), but was found essentially unchanged.

The relative density of the undeformed sample is 94.9%. The C-1000°C-15 min sample is with 94.4% almost identical. Meanwhile, both density and elastic modulus of the C-1050°C samples change with increasing the creep time, which is ascribed to hot forging effects and elucidates the involvement of diffusion-based defects. An uniaxial compressive creep test is in terms of sintering a hot forging process and can lead to enhanced densification.[37] In contrast, the decrease in density of C-1050°C-30 min sample may be due to formation of cavities and microcracks.[38] The creep strain (plastic part of the true strain) increases with rising temperature, stress, and time. C-1050°C-30 min reaches the highest strain with 1.29%, without showing signs of macroscopic failure. The elastic modulus values are in the range of the work of Trzepieciński and Gromada.[39] The linear relation between elastic modulus und density indicates that the changes in elastic modulus are most likely based on porosity. Microcracks or pores would decrease the elastic modulus more drastically.[40–43] Here all values are similar, which indicate absence of pronounced microcrack formation.

Microstructural changes introduced by creep can create local stress fluctuations[44] and thus influence the microstrains. Changes in the microstrains are reflected by the changing full width at half maxima (FWHM) of the X-ray diffraction peaks. To investigate the microstrains, the FWHM of the Bragg peaks was measured in the cubic phase at temperatures above T_c (T_c = 130°C) [45] so that all peaks

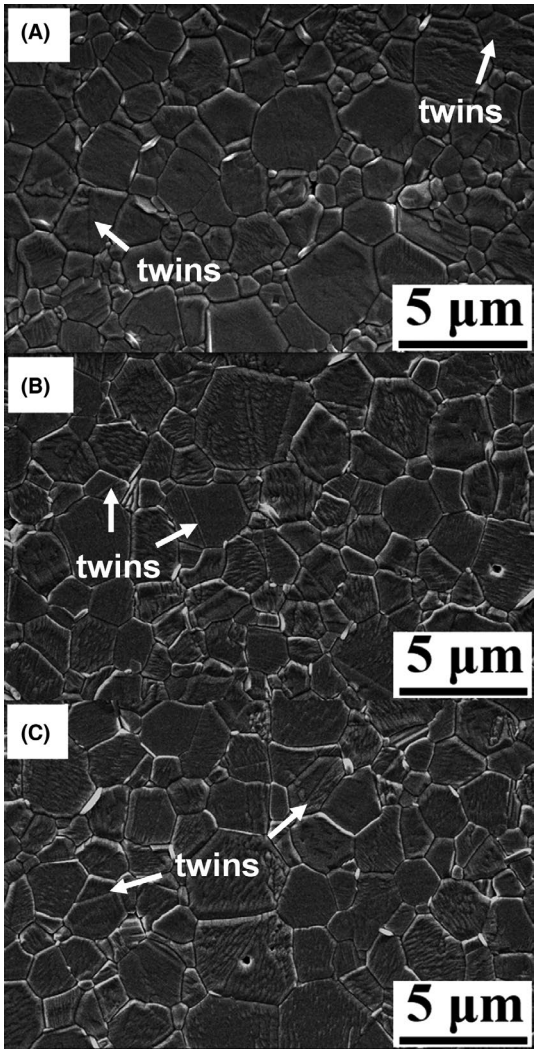

FIGURE 6 SEM images of (A) undeformed BT, (B) C-1000°C-15 min, and (C) C-1050°C-30 min

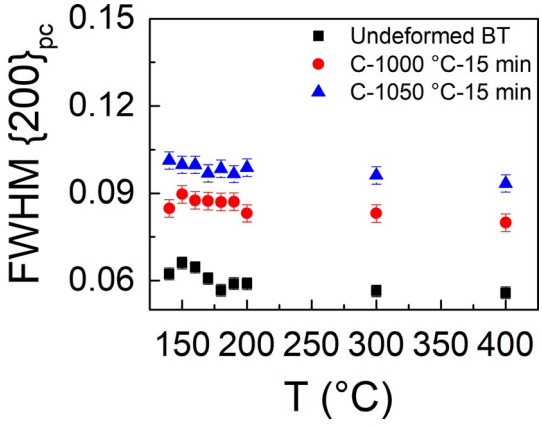

FIGURE 7 X-ray diffraction provided the full width at half maxima (FWHM), exemplarily depicted here for the $\{200\}_{pc}$ peak above the Curie temperature [Color figure can be viewed at wileyonlinelibrary.com]

have become singlets (S1) and are free from tetragonal distortion and domain texturing. Compared to undeformed BT, the FWHM of the {200} peak increases significantly for the C-1000°C-15 min and C-1050°C-15 min samples (Figure 7), indicating that creep deformation considerably enhances the microstrains. Also, these strains are stable at least up to 400°C, which was the highest measured temperature. In polycrystalline ceramic samples the microstrains are influenced by several parameters, including dislocations, twinning, grain boundaries, domains, etc.[46] In the present analysis, the amount of twins and the grain size did not change significantly after deformation, while the domains were excluded by performing the measurements above the Curie temperature. These results strongly indicate that the increased FWHM is related to the increased dislocation density in the creeped samples.

More detailed investigations of the influence of the deformation process on the microstructure were carried out with transmission electron microscopy (Figure 8). All samples experienced a ferroelectric domain structure. The visualization of domains depends on grain orientation and tilt angle, therefore domains are not simultaneously visible in every grain. The undeformed sample (Figure 8A,B) exhibits a microstructure with grain boundaries and no evidence of dislocation structures. For the C-1000°C-15 min sample (Figure 8C,D) cavitation at the grain boundary (C) and individual dislocations within grains (D) were identified. Cavitation and dislocations also appear in Figure 8E for the C-1050°C-30 min sample. The dislocations found in the C-1050°C-30 min (Figure 8F) sample feature similar structures as shown by Suzuki et al for polycrystalline $BaTiO_3$ sintered in reduced atmosphere.[47]

Cavitations are evidence for the existence of local stress centers at the grain boundaries, which are most likely caused by grain-boundary sliding.[44,48] If grain-boundary sliding is hindered by the neighbouring grain boundaries, then this results in the formation of local stress centers. Cavitations are formed when the interlocking of the grain boundaries is loosened and the stresses are released. These features appear in both deformed samples, the C-1000°C-15 min sample and in the C-1050°C-30 min sample. Therefore, it is concluded that grain-boundary sliding is at least a secondary creep mechanism in the C-1050°C-30 min sample and most likely a primary creep mechanism in the C-1000°C-15 min sample. The appearance of grain-boundary sliding indicates that the stress exponents (Figure 5) arise due to both dislocation creep contribution and grain-boundary sliding.

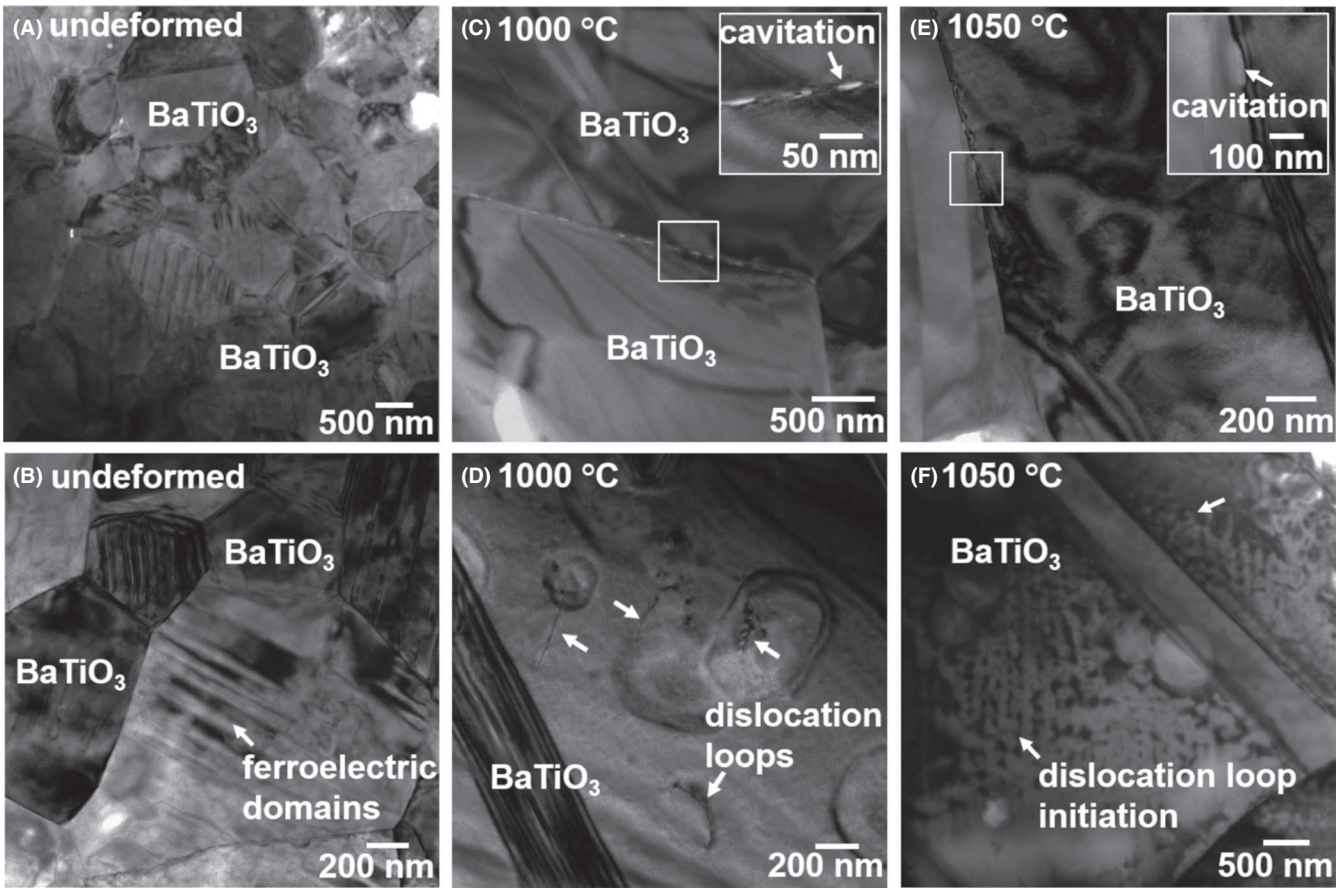

FIGURE 8 TEM bright field images are provided for the undeformed $BaTiO_3$ as an (A) overview image and depict the domain structures in BT (B). In (C) cavitation at a grain boundary and (D) individual dislocations that were initiated are featured for the C-1000°C-15 min sample. The C-1050°C-30 min sample exhibits cavitation at a grain boundary (E) and different types of dislocations (F)

The individual dislocations in Figure 8D and the dislocation structures in (F) verify that it is possible to introduce dislocations by plastic deformation of $BaTiO_3$. Previous TEM analyses have demonstrated that different types of dislocations can be induced in $BaTiO_3$-based materials.[35,47,49–52] Figure 8D reveals typical dislocations loops with scallops along the dislocation line.[50,51] The dislocations in Figure 8F are smaller and occur much more frequently. Suzuki et al argued that these loops arise due to vacancy condensation and require the presence of Schottky defects (eg, V''_{Ba}, V''''_{Ti}, $V^{\bullet\bullet}_{O}$).[47] Additionally, it was proven that dislocations can adorn domain walls[52] and that the density of the dislocation loops can be influenced by oxygen partial pressure.[53]

The domain structure was investigated with piezoresponse force microscopy. The PFM images in Figure 9 display the topography and the lateral amplitude for the undeformed sample (A, B), C-1000°C-15 min (C, D), and C-1050°C-30 min (E, F). For all images BT is in the tetragonal phase, therefore the depicted domain walls are 90° and 180°. The domain size is in the range of 115–154 nm, which is in agreement with the reports by Hoshina et al[54] (100 nm for a grain size of 1.1 μm) and Cao and Randall[55] (150 nm-300 nm for grain sizes of 2 μm-4 μm). Although no significant changes in the domain structure between the samples could be observed by the PFM, a more detailed analysis of the local domain structure in the vicinity of the dislocations should be carried out in the future.

In order to study the effects of creep on dielectric properties, permittivity (Figure 10A) and dielectric loss (Figure 10B) as a function of temperature were quantified for the undeformed and deformed BT at 1 kHz (Figure 10). For a fine grain size of (1–2) μm, a permittivity in the range of 3000 was expected at room temperature.[56] Compared to undeformed BT, differences for deformed BT are observed both at room temperature as well as around the Curie temperature: (a) permittivity at room temperature increases; (b) permittivity at Curie temperature (T_c) decreases; (c) the T_c peak is broader for the deformed samples and the peak is consistently shifted to higher temperatures; (d) the changes in tanδ are small for all the samples except C-1050°C-30 min, which has slightly higher tanδ. The permittivity peak broadening at T_c could be caused by enhanced microstrains, which were observed to increase after deformation (Figure 7).

The different processes that contribute to the sample's resistance can be elucidated using impedance spectroscopy. In Figure 11 the imaginary part of the impedance (-Z'') is plotted against the real part (Z'). Two processes are identified, which can be attributed to low bulk and high grain-boundary resistance.[57] The bulk resistance does not change significantly due to deformation. However, the grain-boundary resistance

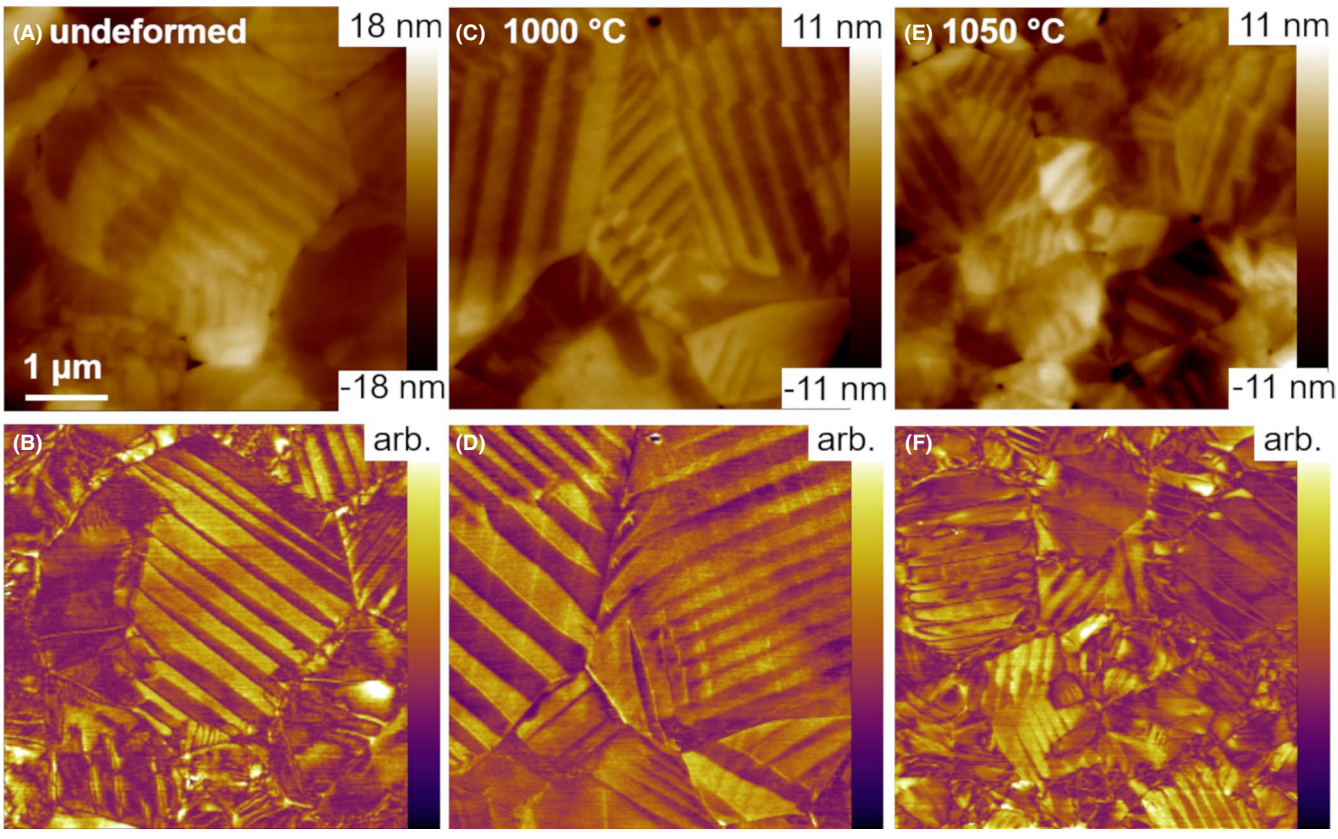

FIGURE 9 Piezoresponse force microscope images of the topography (A, C, E) and the lateral amplitude (B, D, F) for an undeformed sample (A, B), C-1000°C-15 min sample (C, D), and C-1050°C-30 min sample (E, F). The scales for the lateral amplitude and the height difference of the topography are on the right, respectively [Color figure can be viewed at wileyonlinelibrary.com]

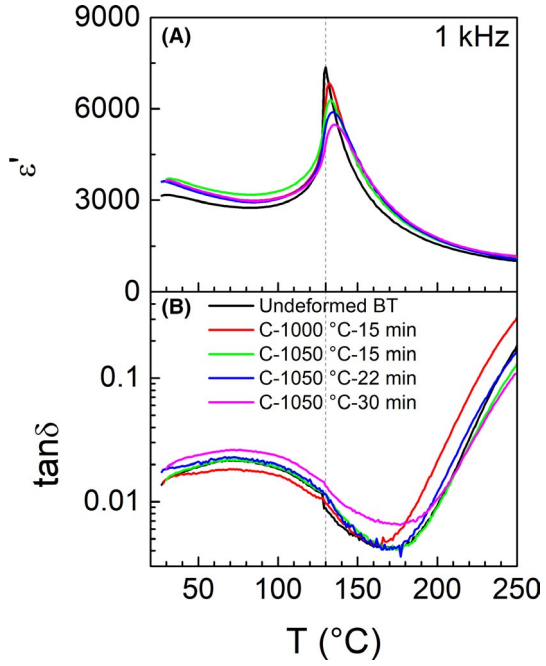

FIGURE 10 (A) Permittivity and (B) loss as function of temperature. The 130°C is marked with a dashed line [Color figure can be viewed at wileyonlinelibrary.com]

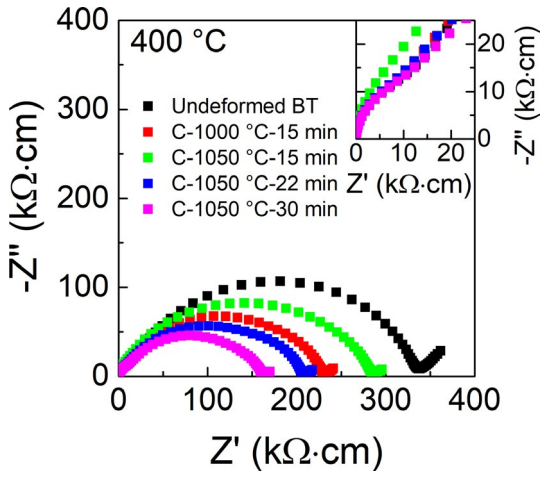

FIGURE 11 Impedance plot for undeformed and deformed BT samples at 400°C [Color figure can be viewed at wileyonlinelibrary.com]

of deformed samples, for example, C-1050°C-30 min, is decreased by a factor of two compared to undeformed BT. These results indicate that the local changes due to creep have a higher influence on the electrical properties of the grain boundaries than the bulk properties. This may be attributed to grain-boundary sliding during deformation, which needs to be considered in addition to diffusion creep and dislocation creep. Local stress centers and cavitations (Figure 8) at the grain boundaries can influence the defect chemistry and, as a consequence, enhance the conductivity of the grain boundaries of the deformed samples. Adepalli et al[8] have found that

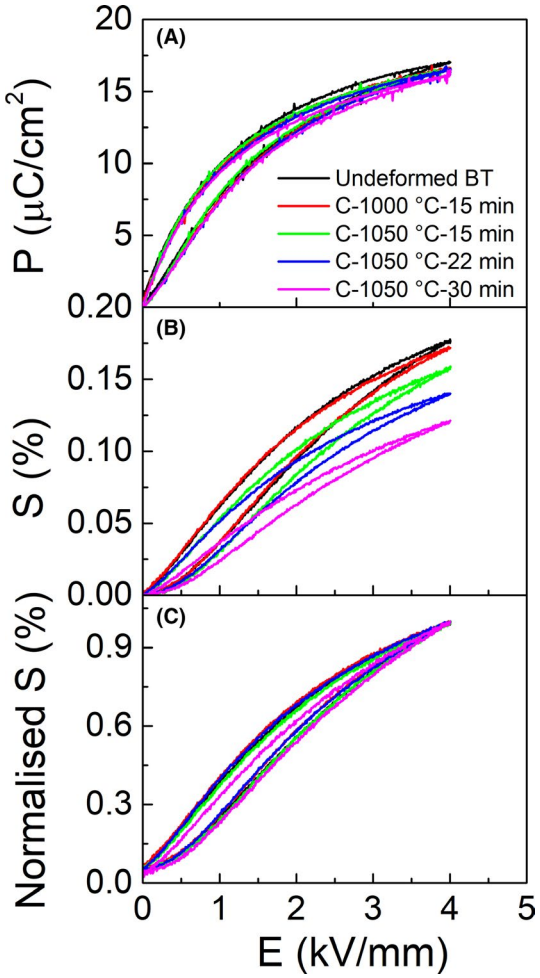

FIGURE 12 Unipolar polarization (A), strain (B), and normalized strain (C) [Color figure can be viewed at wileyonlinelibrary.com]

also charged dislocations influence the point defect chemistry in TiO_2 and therefore influence the conductivity as well.

Unipolar polarization and strain loops as function of applied electric field are provided in Figure 12. Since deformation did not influence the material's bulk crystallographic structure, the intrinsic contribution to strain (converse piezoelectric effect) is assumed to be the same for all the samples. The observed changes can therefore be directly related to the changes in the extrinsic contributions, that is, the domain contribution. After creep, polarization is only slightly affected (Figure 12A), but the strain decreases notably (Figure 12B). The PFM analysis revealed no changes in the domain size after deformation, which could indicate that the observed reduced extrinsic response could be related to the reduced mobility of ferroelastic domain walls. A decrease in strain could therefore be an indication for electromechanical hardening.[4,58] The observation that the ferroelastic response is influenced stronger than the polarization can be rationalized by assuming that switching/movement of 90° domains is affected to a larger degree than switching of 180° domains. In

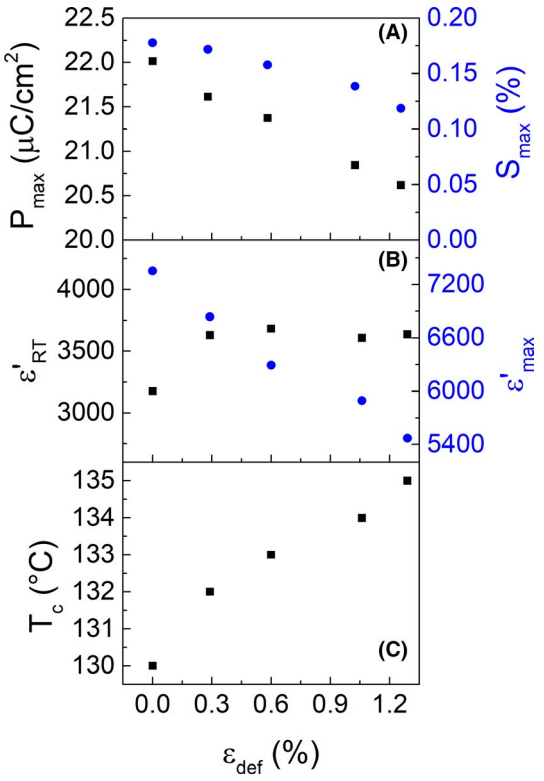

FIGURE 13 (A) Maximum polarization (P_{max}) and strain (S_{max}), (B) permittivity at room temperature (ε'_{RT}) and maximum permittivity (ε'_{max}), and (C) shift in Curie temperature (T_c), as function of creep strain (ε_{def}) [Color figure can be viewed at wileyonlinelibrary.com]

order to compare the hysteresis of the strain, the strain was normalized to maximum strain of the undeformed sample (Figure 12C). After creep, the hysteresis of the strain decreases by 30%, supporting the hypothesis that 90° domain switching is hindered.

Figure 13 summarizes the maximum polarization (P_{max}) and strain (S_{max}), permittivity at room temperature (ε'_{RT}), maximum permittivity (ε'_{max}), and Curie temperature (T_c) as a function of creep strain (ε_{def}). P_{max} is reduced by 10% and S_{max} is reduced by 30% with increasing the creep strain. Note that cavitations present in the largely plastically deformed samples can lead to a reduction of the local electric field in the bulk, as previously demonstrated for piezoceramics with anisometric pores.[59] As a consequence also the electromechanical strain and polarization are reduced; however, this effect seems to be rather small. ε'_{RT} first increases with increasing creep strain and then slightly decreases, with a maximum value for the 0.6% deformed sample (C-1050°C-15 min). The increase of ε'_{RT} is possibly related to the enhanced stress distribution and the decrease of ε'_{RT} may be due to the presence of cavitation in C-1050°C-22 min and C-1050°C-30 min. In comparison with ε'_{RT}, ε'_{max} monotonously decreases while T_c increases with increasing plastic deformation. The enhanced stress distribution and enhanced defect density lead to a local T_c variation, and therefore also ε'_{max} is reduced. The effect of enhanced Curie temperature by 5°C appears high. It is of comparable magnitude to the effect of uniform compressive stresses of 100 MPa-200 MPa, which was demonstrated to enhance the Curie temperature in polycrystalline $BaTiO_3$ by 5°C-10°C.[60]

4 | CONCLUSIONS

We have outlined a methodology to study the impact of creep deformation on the dielectric, ferroelectric, and piezoelectric properties of polycrystalline $BaTiO_3$. The creep exponents display strong variation with experiments and a creep strain of about 1% could be achieved with limited microstructural damage. With increasing plastic deformation, a decrease in polarization of about 10%, a reduction of the electromechanical strain by 30%, and an increase of T_c by 5°C were achieved. TEM analysis revealed noticeable microstructural changes, for example, appearance of dislocations and cavitations, while X-ray diffraction showed an increase in residual stress and microstrains, both of which can be related to changes in permittivity and electrical conductivity. Among these, the reduction in the strain hysteresis and the increase in Curie temperature may prove useful for ferroelectric applications.

ACKNOWLEDGMENTS

The authors are indebted to the Deutsche Forschungsgemeinschaft for funding this work under No. 398795637. PR thanks the support of National Natural Science Foundation (51972265) and Key Research and Development Program (Program No. 2019KW-025) of Shaanxi province of China. PR also thanks Lalitha KV for providing $BaTiO_3$ powders.

ORCID

Marion Höfling https://orcid.org/0000-0002-9387-9610
Jurij Koruza https://orcid.org/0000-0002-0258-6709
Till Frömling https://orcid.org/0000-0002-8827-1926
Lukas Porz https://orcid.org/0000-0003-3163-085X
Jürgen Rödel https://orcid.org/0000-0002-8975-7741

REFERENCES

1. Cai WN, William D. Imperfections in crystalline solids. Cambridge, UK: Cambridge University Press; MRS Materials Research Society; 2016.
2. Uchino K, Zheng JH, Chen YH, Du XH, Ryu J, Gao Y, et al. Loss mechanisms and high power piezoelectrics. J Mater Sci. 2006;41(1):217–28.

3. Arlt G, Hennings D, Dewith G. Dielectric properties of fine-grained barium titanate ceramics. J Appl Phys. 1985;58(4):1619–25.
4. Lalitha KV, Riemer LM, Koruza J, Rödel J. Hardening of electromechanical properties in piezoceramics using a composite approach. Appl Phys Lett. 2017;111(2):022905.
5. Adepalli KK, Kelsch M, Merkle R, Maier J. Influence of line defects on the electrical properties of single crystal TiO_2. Adv Funct Mater. 2013;23(14):1798–806.
6. Marrocchelli D, Sun LX, Yildiz B. Dislocations in $SrTiO_3$: easy to reduce but not so fast for oxygen transport. J Am Chem Soc. 2015;137(14):4735–48.
7. Szot K, Rodenbücher C, Bihlmayer G, Speier W, Ishikawa R, Shibata N, et al. Influence of islocations in transition metal oxides on selected physical and chemical properties. Crystals. 2018;8(6):241.
8. Adepalli KK, Kelsch M, Merkle R, Maier J. Enhanced ionic conductivity in polycrystalline TiO_2 by "one-dimensional doping". Phys Chem Chem Phys. 2014;16(10):4942–51.
9. Adepalli KK, Yang J, Maier J, Tuller HL, Yildiz B. Tunable oxygen diffusion and electronic conduction in $SrTiO_3$ by dislocation-induced space charge fields. Adv Funct Mater. 2017;27(22):1700243.
10. Whitworth RW. Charged dislocations in ionic crystals. Adv Phys. 1975;24(2):203–304.
11. Dam B, Huijbregtse JM, Klaassen FC, van der Geest RC, Doornbos G, Rector JH, et al. Origin of high critical currents in $YBa_2Cu_3O_7$-delta superconducting thin films. Nature. 1999;399(6735):439–42.
12. Kim SI, Lee KH, Mun HA, Kim HS, Hwang SW, Roh JW, et al. Dense dislocation arrays embedded in grain boundaries for high-performance bulk thermoelectrics. Science. 2015;348(6230):109.
13. Kontsos A, Landis CM. Computational modeling of domain wall interactions with dislocations in ferroelectric crystals. Int J Solids Struct. 2009;46(6):1491–8.
14. Gao P, Nelson CT, Jokisaari JR, Baek S-H, Bark CW, Zhang YI, et al. Revealing the role of defects in ferroelectric switching with atomic resolution. Nat Commun. 2011;2(591):1–6.
15. Gaillard Y, Macias AH, Muñoz-Saldaña J, Anglada M, Trapaga G. Nanoindentation of $BaTiO_3$: dislocation nucleation and mechanical twinning. J Phys D-Appl Phys. 2009;42(8):085502.
16. Scholz T, McLaughlin KK, Giuliani F, Clegg WJ, Espinoza-Beltrán FJ, Swain MV, et al. Nanoindentation initiated dislocations in barium titanate ($BaTiO_3$). Appl Phys Lett. 2007;91(6):062903.
17. Oshima Y, Nakamura A, Matsunaga K. Extraordinary plasticity of an inorganic semiconductor in darkness. Science. 2018;360(6390):772–4.
18. Langdon TG. Deformation mechanism maps for applications at high temperatures. Ceramurgia Int. 1980;6(1):11–8.
19. Chokshi AH. Diffusion creep in oxide ceramics. J Eur Ceram Soc. 2002;22(14–15):2469–78.
20. Coble RL. A model for boundary diffusion controlled creep in polycrystalline materials. J Appl Phys. 1963;34(6):1679–82.
21. Nabarro FRN. Report of a conference on the strength of solids. London: Physical Society, 1948; p. 75–90.
22. Herring C. Diffusional viscosity of a polycrystalline solid. J Appl Phys. 1950;21(5):437–45.
23. Chang HC, Grant NJ. Mechanism of intercrystalline fracture. Trans Am Inst Min Metall Eng. 1956;206(5):544–51.
24. Pelleg J. Mechanical properties of ceramics. Cham: Springer, 2014; p. 765.
25. Wachtman JB, Cannon WR, Matthewson MJ. Mechanical properties of ceramics. Hoboken: John Wiley & Sons, Inc., 2009; p. 479.
26. Blum W. High-temperature deformation and creep of crystalline solids. Materials Science and Technology. Hoboken: Wiley-VCH Verlag GmbH & Co. KGaA. 2006; p. 360–403.
27. Blum W, Eisenlohr P, Breutinger F. Understanding creep - a review. Metall Mater Trans A. 2002;33(2):291–303.
28. Cannon WR, Langdon TG. Creep of ceramics.1. Mechanical characteristics. J Mater Sci. 1983;18(1):1–50.
29. Cannon WR, Langdon TG. Creep of ceramics 2. An examination of flow mechanisms. J Mater Sci. 1988;23(1):1–20.
30. Kassner ME, Perez-Prado MT, Vecchio KS, Wall MA. Determination of internal stresses in cyclically deformed copper single crystals using convergent-beam electron diffraction and dislocation dipole separation measurements. Acta Mater. 2000;48(17):4247–54.
31. Wilkinson DS. Creep mechanisms in multiphase ceramic materials. J Am Ceram Soc. 1998;81(2):275–99.
32. Acosta M, Novak N, Rojas V, Pate S, Vaish R, Koruza J, et al. BaTiO3-based piezoelectrics: Fundamentals, current status, and perspectives. Appl Phys Rev. 2017;4(4):041305.
33. Muñoz-Saldaña J, Schneider GA, Eng LM. Stress induced movement of ferroelastic domain walls in $BaTiO_3$ single crystals evaluated by scanning force microscopy. Surf Sci. 2001;480(1–2):L402–L410.
34. Chakrabarty J. Applied plasticity. New York, NY: Springer, 2010; p. 755.
35. Beauchesne S, Poirier JP. Creep of barium bitanate perovskite: a contribution to a systematic approach to the viscosity of the lower mantle. Phys Earth Planet Inter. 1989;55(1):187–99.
36. Schmelz H, Thomann H. Grain-growth in BaTiO3 ceramics.1. Evidence of twinning and exaggerated grain-growth below the eutectic temperature. Am Ceram Soc Bull. 1982;61(8):813.
37. Zuo RZ, Aulbach E, Bordia RK, Rödel J. Critical evaluation of hot forging experiments: case study in alumina. J Am Ceram Soc. 2003;86(7):1099–105.
38. Yousef SG, Rödel J, Fuller ER Jr, Zimmermann A, El-Dasher BS. Microcrack evolution in alumina ceramics: experiment and simulation. J Am Ceram Soc. 2005;88(10):2809–16.
39. Trzepieciński T, Gromada M. Characterization of mechanical properties of barium titanate ceramics with different grain sizes. Materials Science-Poland. 2018;36(1):151–6.
40. Zimmerman R. The effect of microcracks on the elastic moduli of brittle materials. J Mater Sci Lett. 1985;4:1457–60.
41. Asmani M, Kermel C, Leriche A, Ourak M. Influence of porosity on Young's modulus and Poisson's ratio in alumina ceramics. J Eur Ceram Soc. 2001;21(8):1081–6.
42. Budiansky B, Oconnell RJ. Elastic-moduli of a cracked solid. Int J Solids Struct. 1976;12(2):81–97.
43. Kachanov M. Effective elastic properties of cracked solids: critical review of some basic concepts. Appl Mech Rev. 1992;45(8):304–35.
44. Watanabe T. Grain boundary sliding and stress concentration during creep. Metall Trans A. 1983;14(3):531–45.
45. Jaffe B, Cook WR, Jaffe H. Piezoelectric ceramics. London: Academic Press, 1971; p. 317.
46. Ungár T. Microstructural parameters from X-ray diffraction peak broadening. Scr Mater. 2004;51(8):777–81.
47. Suzuki T, Ueno M, Nishi Y, Fujimoto M. Dislocation loop formation in nonstoichiometric (Ba, Ca)TiO_3 and $BaTiO_3$ ceramics. J Am Ceram Soc. 2001;84(1):200–6.
48. Perry AJ. Cavitation in creep. J Mater Sci. 1974;9(6):1016–39.

49. Eibl O, Pongratz P, Skalicky P, Schmelz H. Dislocations in $BaTiO_3$ ceramics. Phys Status Solidi A. 1988;108(2):495–502.
50. Doukhan N, Doukhan JC. Dislocations in perovskites $BaTiO_3$ and $CaTiO_3$. Phys Chem Minerals. 1986;13(6):403–10.
51. Cheng SY, Ho NJ, Lu HY. Dissociation of the <001> dislocations and their interactions with dislocation loops in tetragonal $BaTiO_3$. J Am Ceram Soc. 2006;89(5):1659–67.
52. Wu YC, Chen CY, Lu HY, McCauley DE, Chu MSH. Dislocation loops in pressureless-sintered undoped $BaTiO_3$ ceramics. J Am Ceram Soc. 2006;89(7):2213–9.
53. Metzmacher C, Albertsen K. Microstructural investigations of barium titanate-based material for base metal electrode ceramic multilayer capacitor. J Am Ceram Soc. 2001;84(4):821–6.
54. Hoshina T. Size effect of barium titanate: fine particles and ceramics. J Ceram Soc Jpn. 2013;121(1410):156–61.
55. Cao W, Randall CA. Grain size and domain size relations in bulk ceramic ferroelectric materials. J Phys Chem Solids. 1996;57(10):1499–505.
56. Buessem WR, Cross LE, Goswami AK. Effect of two-dimensional pressure on the permittivity of fine- and coarse-grained barium titanate. J Am Ceram Soc. 1966;49(1):36–9.
57. Irvine JTS, Sinclair DC, West AR. Electroceramics: characterization by impedance spectroscopy. Adv Mater. 1990;2(3):132–8.
58. Li F, Wang L, Jin L, et al. Piezoelectric activity in perovskite ferroelectric crystals. IEEE Trans Ultrason Ferroelectr Freq Control. 2015;62(1):18–32.
59. Khachaturyan R, Zhukov S, Schultheiß J, et al. Polarization-switching dynamics in bulk ferroelectrics with isometric and oriented anisometric pores. J Phys D: Appl Phys. 2016;50(4):045303.
60. Schader FH, Aulbach E, Webber KG, Rossetti GA. Influence of uniaxial stress on the ferroelectric-to-paraelectric phase change in barium titanate. J Appl Phys. 2013;113(17):174103.

SUPPORTING INFORMATION

Additional supporting information may be found online in the Supporting Information section.

How to cite this article: Ren P, Höfling M, Koruza J, et al. High temperature creep-mediated functionality in polycrystalline barium titanate. *J Am Ceram Soc*. 2020;103:1891–1902. https://doi.org/10.1111/jace.16881